Stieltjes imaging method for molecular Auger transition rates: Application to the Auger spectrum of water

Vincenzo Carravetta
Istituto di Chimica Quantistica ed Energetica Molecolare del Consiglio Nazionale delle Ricerche, Via Risorgimento 35, 56100 Pisa, Italy

Hans Ågren
Institute of Quantum Chemistry, University of Uppsala, P.O.B. 518, S-75120 Uppsala, Sweden
(Received 3 June 1986)

A Stieltjes imaging method for the calculation of molecular Auger transition rates within Wentzel's ansatz is devised and numerically applied to the Auger emission spectrum of water vapor. Continuum orbitals are solved in the anisotropic field of the doubly ionized molecule using an extended set of L^2 integrable basis functions. The effects on the Auger rates of nonorthogonality between the bound orbitals (electronic relaxation) as well as of hole mixing due to the interaction of the residual final states are numerically evaluated and discussed. Comparisons are made with a previously devised atomic decomposition scheme and with experiment. The summation of Auger channel rates gives a value of 0.15 eV for the lifetime broadening of the core-hole state of water.

I. INTRODUCTION

The theory of the Auger effect has lately been much advanced and is now put in the framework of multichannel resonance scattering.[1] The implementation of Auger theory for molecular many-electron systems has, however, exclusively been confined to Wentzel's ansatz.[2] This ansatz is obtained from Fermi's golden rule in the limit of zero frequency of the external field, with the Auger decay approximated as a two-step process in which interaction with photoelectrons or other collisional products is neglected. A derivation of Wentzel's ansatz for wave functions built on mutually nonorthogonal sets of orbitals and with interacting continuum channels was given by Howat, Åberg, and Goscinski[3] and extended to initial- and final-state many-particle wave functions by Manne and Ågren,[4] who, however, retained a single-channel description for the outgoing electron. Other methods within the framework of Wentzel's ansatz are the many-body perturbation method of Kelly,[5] and the two-particle Green's-functions method of Liegener.[6]

While the calculation of transition energies can be obtained with high accuracy with computer codes for bound eigenstates, molecular Auger intensities have been carried out with several simplifying assumptions. The common way to proceed has been to assume a single-particle approximation for the initial state and to have the Auger intensities guided by the convolution of expansion coefficients for the main hole-configuration functions in the final-state wave functions (generalized Auger overlap amplitudes[4] or pole strengths of the particle-particle Green's functions[6]) with atomically decomposed transition moments.[7–9] For covalent, electron-rich molecules, the molecular orbital picture is known to break down for the description of the final two-hole states of the Auger transitions.[10] This leads to a rather complex intensity analysis with considerations of intensity-borrowing and interference effects. The main bottleneck lies, however, in the definition of the atomic decomposition of transition rates which, being based on population analysis, only can provide semiquantitative accuracy. Calculations of Auger moments from continuum orbitals expanded as spherical waves in one-center expanded potentials have been carried out by Faegri and Kelly for HF (Ref. 11) and by Hihashi, Hiroike, and Nakajima for CH_4 (Ref. 12). Except for these two investigations no attempts to go beyond the simple decomposition scheme have been made, and its limitation has never been fully explored.

Auger rate calculations using Wentzel's ansatz, even in the form for frozen-orbital and one-particle wave functions, are difficult to carry out for molecules. As for theoretical calculations describing other molecular bound-continuum transitions this is because of the description of the final state. The many-electron continuum is generally approximated by an antisymmetrized product of a fixed target function for the molecular ion and a continuum orbital for the outgoing electron.[13] The calculation of an accurate molecular continuum orbital is complicated by the anisotropy of the ionic field, and is generally carried out by computational techniques that essentially can be divided into scattered-wave and L^2 techniques.[13] In L^2 methods the continuum orbital is projected on an integrable-functions basis set and a complete *ab initio* approach is used. The main advantage with these more rigorous methods is that they allow for varying levels of approximation in the calculations that, besides, can be carried out by well-established computer codes already developed to treat bound-state problems. Among the other L^2 methods suggested in the last few years, the so-called Stieltjes imaging procedure[14,15] received the largest attention and has been applied quite extensively to the calculation of molecular photoionization cross sections.[11–19]

Present continuum-orbital calculations are performed in the static-exchange[13] approximation for the doubly charged ionic field and neglecting the coupling with the rotational and vibrational motions. Bound electronic eigenfunctions of the single and doubly ionized ions, at the ground-state equilibrium geometry, are described as single Slater determinants by using a large basis set of Slater functions [Slater-type orbitals (STO's)] centered on the O nucleus. Each of the several double-hole final states is considered to identify an independent channel and correspondingly a single-particle Hamiltonian for the continuum orbitals. In order to get a discretized representation of the continuous spectrum of this Hamiltonian, a large number of special oscillating functions, already introduced by one of us,[18–20] is added to standard Slater functions. The correct normalization per unit energy range of the continuum orbitals is obtained by a proposed Stieltjes imaging procedure. A better description of the initial and final states can be obtained by the inclusion of electronic relaxation. This gives rise to nonorthogonality problems that in the present paper have been carefully investigated for a few of the most important channels.

The essential details of the method are presented in Sec. II. In Sec. III we describe the computational procedure for generating the discrete representation of the continuum functions. In Sec. IV we present and discuss results for partial-wave and mixed-wave approximations and for generalization to bound-state wave functions which intrinsically contain relaxation (nonorthogonality) and configuration-interaction effects. Results are compared with the previously employed atomic decomposition scheme and with the experimental spectrum, and in Sec. IV C a value for the lifetime broadening of the core-hole state is derived.

II. METHOD

To give a formal justification for the proposed Stieltjes imaging method of Auger rates, we recall that the lowest-order contribution to the correlation energy of an inner-shell hole (h) can be written as (see Kelly[21,22])

$$E_h^{(2)}=\sum_{(x\geq y)} E_{hxy}^{(2)} ,$$
$$E_{hxy}^{(2)}=\sum_{\nu}^{\text{disc}} \frac{|\langle xy||\nu h\rangle|^2}{\varepsilon_x+\varepsilon_y-\varepsilon_\nu-\varepsilon_h}+\int_0^\infty dE \frac{|\langle xy||\nu(E)h\rangle|^2}{\varepsilon_x+\varepsilon_y-E-\varepsilon_h} , \tag{1}$$

where the two final-state hole, the initial core holes, and the excited orbital are denoted by x, y, h, and ν, respectively. The excited orbital energy takes discrete ε_ν and continuous (E) values; the continuum orbital $\nu(E)$ is considered to be normalized per unit energy interval. The Auger effect occurs for the singularities $E=\varepsilon_x+\varepsilon_y-\varepsilon_h$ of the various functions $E_{hxy}^{(2)}$, and the Auger decay rates are given by the residues of these singularities.[21] The integral over the continuum-orbital energy E can be written in the following way considering the continuum orbital ν normalized per unit K interval [this normalization differs by a factor of $\sqrt{(2/\pi)}$ from that adopted by Kelly[21,22]]:

$$\int_0^\infty dK \frac{|\langle xy||\nu(K)h\rangle|^2}{\varepsilon_x+\varepsilon_y-\frac{1}{2}K^2-\varepsilon_h} . \tag{2}$$

A direct comparison with the polarizability expression,

$$\alpha(\omega)=\int_0^\infty \frac{df(\varepsilon)}{\varepsilon^2-\omega^2} ,$$
$$\frac{df(\varepsilon)}{d\varepsilon}=\sum_i^{\text{disc}} f_i\delta(\varepsilon-\varepsilon_i)+g(\varepsilon) , \tag{3}$$

which generally is assumed to be the formal justification[15] for the application of the Stieltjes imaging technique to the calculation of photoionization cross sections, shows that the integral in Eq. (2) is a Stieltjes integral with K and $|\langle xy||\nu(K)h\rangle|^2$ taking the places that in the polarizability expression are those of the energy (ε_i) and of the oscillator strength $df(\varepsilon)/d\varepsilon$ distribution, respectively. A discrete "spectrum" $\{K, |\langle xy||\nu h\rangle|^2\}$, obtained, for instance, in the way described below from L^2 integrable orbitals, thus forms a basis for a Stieltjes construction of a "K-normalized" continuous function,

$$Z_{hxy}(K)=|\langle xy||\nu(K)h\rangle|^2 . \tag{4}$$

Differently from the photoionization process, where we are interested in the imaginary part of the polarizability on a continuous range for the photon energy, we are, for the Auger process, interested just in one value of the function $Z_{hxy}(K)$ corresponding to the resonance energy of the considered channel. The Auger decay rate can be written as

$$\Gamma_{hxy}=\frac{2\pi}{K_0}Z_{hxy}(K_0) ,$$
$$K_0=[2(\varepsilon_x+\varepsilon_y-\varepsilon_h)]^{1/2} . \tag{5}$$

According to the analogies mentioned above the numerical procedure to implement the Stieltjes imaging of the discretized spectrum is the same described in details in previous papers.[18,19]

Using the static-exchange independent-channel approximation, more extensively described in previous papers,[18,19] the initial state was approximated by the relaxed $1s$-hole self-consistent-field (SCF) wave function $|\Psi_{1s}\rangle$ and the continuum doublet final states by coupling a double-hole (indices x and y) singlet or triplet projected combination of determinants, built from the neutral ground-state orbitals, to a continuum orbital (index ε) that is variationally determined in the ionic field,

$$|\psi_{xy\varepsilon}^S\rangle=\frac{1}{\sqrt{2}}\{\hat{a}^\dagger_{\varepsilon_\alpha}\hat{a}_{x_\beta}\hat{a}_{y_\alpha}-\hat{a}^\dagger_{\varepsilon_\alpha}\hat{a}_{x_\alpha}\hat{a}_{y_\beta}\}|\psi_{GS}^N\rangle , \tag{6}$$

$$|\psi_{xy\varepsilon}^T\rangle=\frac{1}{\sqrt{6}}\{2\hat{a}^\dagger_{\varepsilon_\beta}\hat{a}_{y_\beta}\hat{a}_{x_\beta}+\hat{a}^\dagger_{\varepsilon_\alpha}\hat{a}_{y_\beta}\hat{a}_{x_\alpha}+\hat{a}^\dagger_{\varepsilon_\alpha}\hat{a}_{y_\alpha}\hat{a}_{x_\beta}\}|\psi_{GS}^N\rangle . \tag{7}$$

Here S and T refer to the singlet and triplet parent ionic states. From the four valence orbitals of H_2O, $2a_1$, $3a_1$, $1b_2$, and $1b_1$, 16 different double-hole ion final states can be obtained, corresponding to 16 Auger decay channels. The final-state frozen orbitals, obtained by an SCF calcu-

lation for the neutral molecular ground state, were used to build, for each channel, the outgoing electron Hamiltonian having the following expressions:

$$h_{xy}^{S}=\hat{T}+\hat{V}_n+\sum_{i\ (\neq x,y)}^{\text{occ}}(2\hat{J}_i-\hat{K}_i)$$
$$+(\hat{J}_x+\hat{J}_y-1/2\hat{K}_x-1/2\hat{K}_y)(1-\delta_{xy}) \tag{8a}$$

for double-hole singlet coupling (S) or

$$h_{xy}^{T}=\hat{T}+\hat{V}_n+\sum_{i\ (\neq x,y)}^{\text{occ}}(2\hat{J}_i-\hat{K}_i)$$
$$+(\hat{J}_x+\hat{J}_y+1/2\hat{K}_x+1/2\hat{K}_y) \tag{8b}$$

for double-hole triplet coupling (T). Here $\hat{T}$, $\hat{V}$, $\hat{J}$, and $\hat{K}$ denote the kinetic energy, nuclear attraction, Coulomb, and exchange operators, respectively. A discretized representation of the continuum was then obtained by solving the one-electron eigenvalue problem with the additional constraint of orthogonality between bound and continuum orbitals after projection on a finite basis set of L^2 functions. Using the previously described approximations for the initial and final states, the partial Auger rate corresponding to the channel x,y (S or T) can be expressed as

$$\Gamma_{xy}^{S,T}=2\pi\,|\,\langle\psi_{xy\varepsilon_0}^{S,T}\,|\,\hat{H}-E\,|\,\psi_{1s}^{N-1}\rangle\,|^2\,,$$
$$\varepsilon_0=E-E_{xy}^{N-2} \tag{9}$$

with the continuum final state normalized per unit energy range. The use of different sets of bound orbitals in the initial and final states gives rise to a nonorthogonality problem[3] in the application of Eq. (9). Computed overlaps between different orbitals are less than 0.01 and, as verified for a few channels (see Sec. IV B), the expression (9) can in a first approximation be reduced to the standard Wentzel expressions,

$$\Gamma_{xy}^{S}=\pi[(1s_f x_i\,|\,\varepsilon_0 y_i)+(1s_f y_i\,|\,\varepsilon_0 x_i)]^2\,,$$
$$\Gamma_{2x}^{S}=2\pi(1s_f x_i\,|\,\varepsilon_0 x_i)^2\,, \tag{10}$$
$$\Gamma_{xy}^{T}=3\pi[(1s_f x_i\,|\,\varepsilon_0 y_i)-(1s_f y_i\,|\,\varepsilon_0 x_i)]^2\,,$$

where

$$(ab\,|\,cd)=\int d\mathbf{r}_1\,d\mathbf{r}_2\varphi_a^*(\mathbf{r}_1)\varphi_c^*(\mathbf{r}_2)\frac{1}{r_{12}}\varphi_b(\mathbf{r}_1)\varphi_d(\mathbf{r}_2) \tag{11}$$

and the subscripts i and f indicate the initial- and final-state spatial orbital sets, respectively.

Using the L^2 integrable continuum orbitals obtained by the previously described computational procedure the quantities in Eq. (10) can be calculated for a discrete set of outgoing electron energies ε_i in place of ε_0. In order to evaluate the continuum normalization we applied the above-described Stieltjes imaging technique to the spectrum $\{K_i,\Gamma_i\}$, where $K_i=\sqrt{(2\varepsilon_i)}$ and Γ_i is given by one of the expressions in Eq. (10) depending on the channel considered. By this procedure, the continuous function $Z(K)$ and hence the Auger rate are obtained, cf. Eq. (5).

III. COMPUTATIONAL

The SCF calculations for the ground state and the $1s$ hole have been carried out using a one-center basis set of 37 STO's obtaining total energies of relatively -75.9703 and -56.1736 hartree; STO's with high values of l (up to 6) and m (up to 4) were included in order to get an adequate description of the occupied orbitals close to the hydrogen nuclei. The static-exchange one-particle Hamiltonians, Eqs. (8a) and (8b), were diagonalized by projecting the continuum orbitals on a large basis set including the STO's localized in the molecular region plus radial oscillating functions having the following expression:

$$X_{nlm}(\xi,K,r,\theta,\varphi)=A_n(\xi,K)r^{n-1}e^{-\xi r}\cos(Kr)Y_l^m(\theta,\varphi)\,. \tag{12}$$

It has already been verified[18–20] that these particular functions, which in the one-center expansion yield easily computable expressions for the one- and two-electron integrals, are quite adequate to fit the continuum orbitals. In particular, the presence of the parameter K in (12) allows us to obtain the desired density of eigenvalues in the energy region of interest, which in the Auger process generally corresponds to hundreds of electron volts. This is hardly possible for the commonly used Slater or Gaussian basis sets. In spite of the large extension of the basis set, the redundancy problem is easily avoided because of the particularities of the oscillating functions. The basis sets employed in the present calculation contained some 75 members for each (l,m) partial-wave space (see Sec. IV A). The value of the parameter K in the oscillating functions ranged from 0 to 8 a.u. and was chosen particularly dense in the Auger resonance region ($\Delta K=0.05$ a.u.). Tests, carried out to verify the stability of the results with respect to variations of this basis set, showed negligible variations of the final rates ($<5\%$). The Stieltjes imaging was performed for each discretized spectrum $\{K_i,\Gamma_i\}$ using a variable number of spectral moments ranging from 14 to 30 and then fitting the K-normalized imaged values by a low-order polynomial according to a well-established procedure[18,19] in order to get the continuous function $Z(K)$. Small values of the least-square deviation were in general obtained, showing that the interpolated value of the imaged Γ at the resonance K value was practically independent of the number of spectral moments considered.

We have also performed multiconfiguration SCF (MCSCF) and large scale configuration-interaction (CI) calculations in order to obtain transition energies with high accuracy and to obtain the mixing coefficients of the Auger rates due to final-state discrete interactions (discrete state coupling of the channels, see Sec. IV). The contracted CI program of Siegbahn[23] and the MCSCF program of Jensen and Ågren[24] were used in these calculations. An extended Gaussian basis set including a polarization d function was used (identical to the basis set used in Refs. 25 and 26). The core hole and valence double hole states have a compact character and are therefore known to be well described by such a basis.[10] The obtained SCF ground-state energy agreed within 0.1 a.u. and the $1s$ ΔSCF (separate-state SCF) ionization potential within 0.5 eV with the corresponding quantities computed

TABLE I. Calculations of Auger rates including relaxation (10^{-6} a.u.). A: Frozen final-state bound orbitals. No overlap correction. B: Relaxed final-state bound orbitals. No overlap correction. C: Relaxed final-state bound orbitals. With overlap correction.

Channel	Partial wave	A	B	C
$3a_1^{-2}$	(2,0)	346	369	363
$1b_1^{-2}$	(2,2)	382	385	375
$1b_2^{-2}$	(2,2)	218	234	222

by the one-center expanded Slater basis described above. Computations were carried out for all 16 discrete channels, except for the high-lying $2a_1^{-2}$ state, due to the extended nature of the CI wave function (5×10^4 configurations). This state was addressed in a previous limited "semi-internal" CI (Ref. 26) using an identical basis set (see Table III). The Auger transition energies, reported in Tables I and II. Figs. 1, 2, and 3 are obtained from differences between calculated total energies for ground and the various final states, and normalized to the experimental core-ionization potential of 539.93 eV.[26] In this way the relativistic error from the removal of a core electron is avoided.

The inclusion of several main configuration states in the final-state wave function poses a phase problem for the Auger intensities. In order to obtain the hole-mixing rates in the independent partial-wave approximation a phase relation between the various Auger moments τ_{hxy} and the expansion coefficients [generalized Auger overlap amplitudes (GAOA's)] c_{xy} for the configuration-state functions of the final state must be established [see definitions in Sec. IV, especially Eq. (16)]. The sign of τ_{hxy} depends on the phase of the bound and of the continuum orbitals. By requiring that the continuum orbitals (partial waves) of different channels have the same (positive) sign close to the origin, the relative sign of the Auger moments of different channels was fixed (they are given in parenthesis in Table III). Imposing the same phase for the bound orbitals used in the CI calculations (expanded with Gaussian functions) as for the bound orbitals employed in the Auger moment calculation (expanded in Slater functions), the correct phase relation between τ_{hxy} and c_{xy} could then be established. The main CI coefficients are listed in Table II.

IV. RESULTS AND DISCUSSION

A. Partial and mixed wave rates

Considering that the continuum orbitals can be expressed as linear combinations of spherical harmonics,

$$\varphi_E(r,\theta,\varphi)=\sum_{l,m} c_E^{lm}\phi_E^{lm}(r,\theta,\varphi)$$
$$=\sum_{l,m} c_E^{lm} f_E^{lm}(r)Y_l^m(\theta,\varphi) \quad (13)$$

the discretized spectrum $\{K_i,\Gamma_i\}$ for each independent channel was obtained at two different levels of approximation: neglecting or not the coupling among different partial waves ϕ_E^{lm} due to the anisotropy of the molecular ionic field. The results of the first kind of calculations are reported in Table III where in the first column the 16 channels corresponding to the different double-hole final states are specified. The following columns display the contributions to the Auger decay rates of the different channels from several partial waves, each identified by an (l,m) value. Total partial rates, obtained as summation of the several partial-waves contributions, are presented in the next to last column, while the results obtained by considering explicitly the coupling among different partial

TABLE II. Auger transition energies (eV) and wave functions of final double-hole states of H_2O obtained from open-shell restricted Hartree-Fock (OSRHF) and multireference configuration-interaction (CI) calculations. CI energies obtained from orbitals which are MCSCF optimized over the reference space. The final-state CI wave functions displayed use ground-state Hartree-Fock orbitals. OSRHF energies from Ref. 25.

Channel		Energies (eV) OSRHF	CI	Wave function of final state (CI)
$2a_1^{-2}$	S	451.45	458.31	$0.77\ (2a_1^{-2})$[a]
$2a_1 3a_1$	S	473.46	472.06	$0.077(1b_1^{-2})+0.034(3a_1^{-2})+0.051(1b_2^{-2})+0.877(2a_1 3a_1)+0.053(2a_1^{-2})$
$2a_1 3a_1$	T	480.66	483.48	$0.969(2a_1 3a_1)$
$2a_1 1b_2$	S	467.26	467.57	$0.899(2a_1 1b_2)-0.038(3a_1 1b_2)$
$2a_1 1b_2$	T	478.83	476.57	$0.877(2a_1 1b_2)-0.100(3a_1 1b_2)$
$2a_1 1b_1$	S	474.02	475.66	$0.896(2a_1 1b_1)-0.013(3a_1 1b_1)$
$2a_1 1b_1$	T	482.14	482.14	$0.897(2a_1 1b_1)-0.083(3a_1 1b_1)$
$3a_1^{-2}$	S	496.40	494.55	$-0.183(1b_1^{-2})+0.898(3a_1^{-2})+0.135(1b_2^{-2})+0.082(2a_1 3a_1)+0.078(2a_1^{-2})$
$3a_1 1b_2$	S	493.79	492.14	$0.980(3a_1 1b_2)$
$3a_1 1b_2$	T	496.35	494.42	$0.980(3a_1 1b_2)$
$3a_1 1b_1$	S	499.57	497.96	$0.960(3a_1 1b_1)$
$3a_1 1b_1$	T	502.62	500.67	$0.960(3a_1 1b_1)$
$1b_2^{-2}$	S	488.32	487.39	$-0.050(1b_1^{-2})-0.108(3a_1^{-2})-0.926(1b_2^{-2})+0.125(2a_1^{-2})$
$1b_2 1b_1$	S	495.72	494.42	$0.956(1b_1 1b_2)$
$1b_2 1b_1$	T	497.74	496.37	$0.954(1b_1 1b_2)$
$1b_1^{-2}$	S	500.77	499.39	$0.895(1b_1^{-2})-0.205(3a_1^{-2})-0.039(1b_2^{-2})-0.053(2a_1^{-2})$

[a]The $2a_1^{-2}$ state from semi-internal CI calculation in Ref. 8.

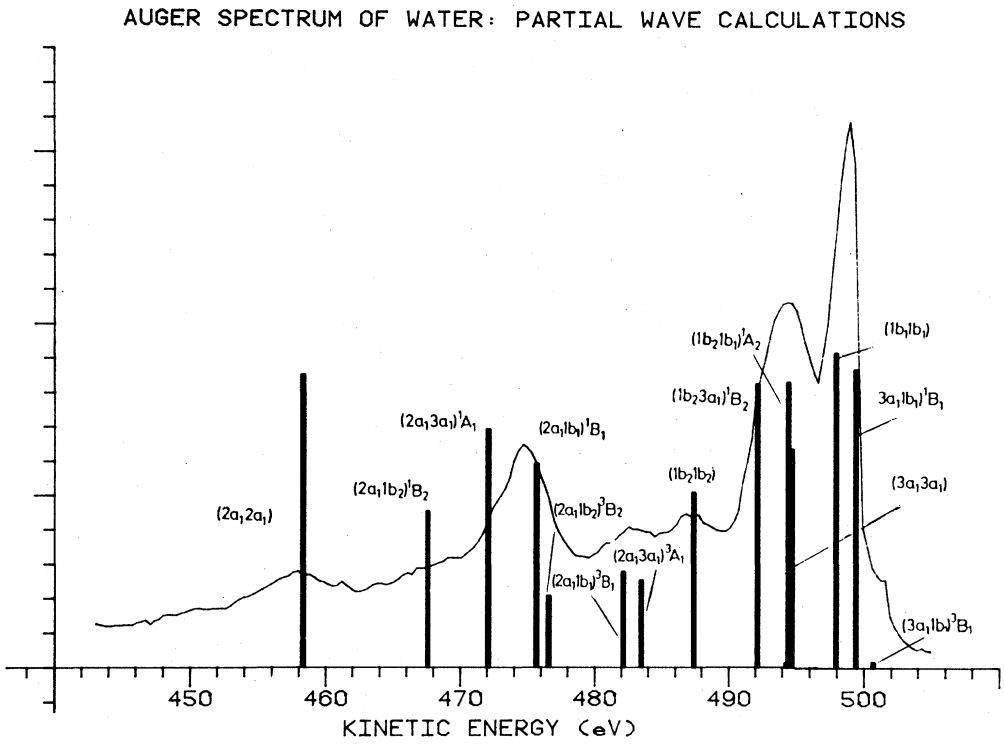

FIG. 1. Auger spectrum of water molecule. Partial-wave intensity calculations.

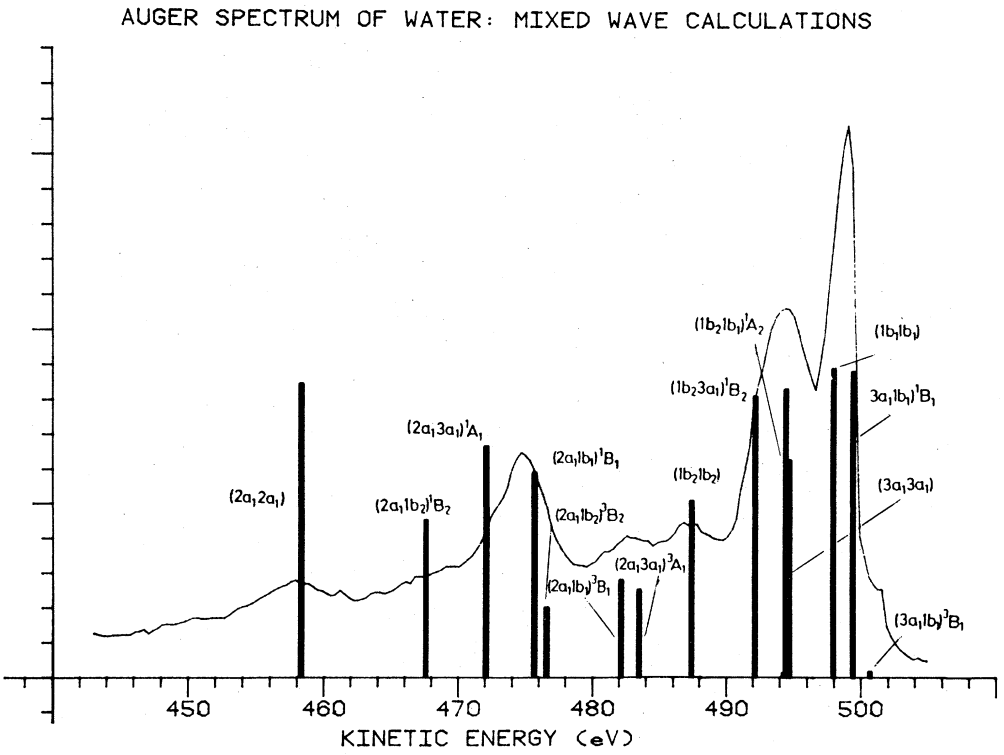

FIG. 2. Auger spectrum of water molecule. Mixed-wave intensity calculations.

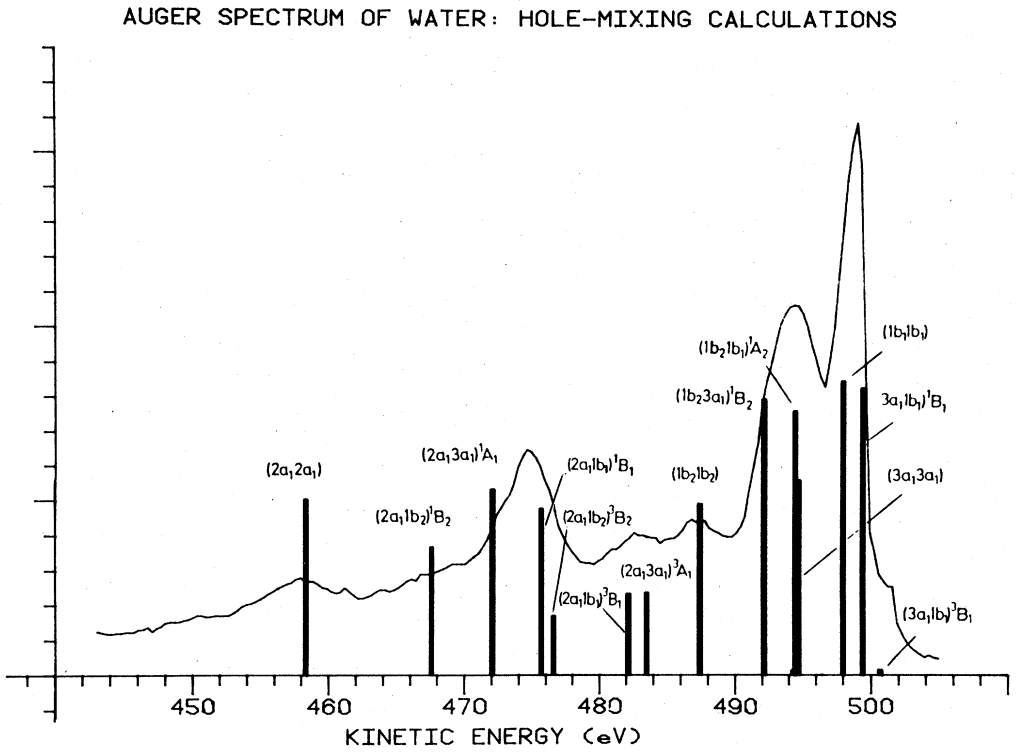

FIG. 3. Auger spectrum of water molecule. Hole-mixing intensity calculations.

waves are collected in the last column. Values of l and m higher than those reported in Table III have been considered, however, they were found to give negligible contributions and are not presented for brevity.

It is clear from Table III that the total channel rates are rather insensitive to the coupling of the partial waves. For transitions pertaining to non-totally-symmetric states this is merely because one partial channel is dominating. Transitions to the $^1A_1$ states have significant contributions from two or three partial channels, which, however, are largely additive. This might find an explanation in that the energy of the Auger electron is very high and in

TABLE III. Partial-wave contributions (l,m) and total Auger decay rates from partial- and mixed-wave calculations for H_2O (10^{-6} a.u.). Signs in parentheses refer to phases of the corresponding partial-wave Auger moments. (The rate is proportional to the square of the moment.)

Channel		(0,0)	(1,−1)	(1,0)	(1,1)	(2,−2)	(2,−1)	(2,0)	(2,1)	(2,2)	Partial-wave sum	Mixed wave
$2a_1^{-2}$	S	(+)581		(−)17				0			598	593
$2a_13a_1$	S	(−)147		(−)322				(+)17			486	467
$2a_13a_1$	T	0		(+)177				0			177	177
$2a_11b_2$	S		(−)305				(+)14				319	318
$2a_11b_2$	T		(+)146				0				146	141
$2a_11b_1$	S				(−)400				(+)16		416	414
$2a_11b_1$	T				(+)195				0		195	197
$3a_1^{-2}$	S	(−)53		(+)47				(+)346		0	446	440
$3a_11b_2$	S		(+)21				(+)559				580	569
$3a_11b_2$	T		(−)9				0				9	9
$3a_11b_1$	S				(+)29				(+)614		643	624
$3a_11b_1$	T				(−)12				0		12	12
$1b_2^{-2}$	S	(−)66		0				(−)74		(−)218	358	358
$1b_21b_1$	S					(+)583					583	583
$1b_21b_1$	T					0					0	0
$1b_1^{-2}$	S	(−)108		0				(−)119		(+)382	609	618
Total											5577	5520

that the anisotropy of the doubly ionized water molecule is relatively small.

Bar spectra representing the results for the partial-wave and mixed-wave calculations are shown in Figs. 1, and 2, respectively, along with the experimental spectrum.[7] In Table IV are the intensities compared with those given by the atomic decomposition scheme.[7] The atomically decomposed values are obtained by weighting atomic radial integrals with relevant linear combination of atomic orbital (LCAO) expansion coefficients for the two valence orbitals that participate in the transition. Two-center cross contributions are then neglected. There is an agreement on the qualitative level between these intensities and the present Stieltjes imaging results. This might be explained by the fact that most of the charge density in water is moved to the oxygen atom. The disagreements between the two sets of values are largest for transitions pertaining to triplet states and for transitions in the low-kinetic-energy end of the spectrum. Triplets generally receive higher intensities in the present calculations, but are still weaker than the corresponding singlets due to the phases of Coulomb and exchange integrals involving the continuum orbital, see Eq. (10). The present partial- or mixed-wave calculations allocate too much intensity in the low-kinetic-energy end which is associated with the strong many-body effects which operate in this region, see discussion in the next paragraph.

B. Role of relaxation and configuration mixing

In this section we discuss the contributions of relaxation and final-state configuration mixing on the Auger rates. We start out from the expression recently derived in Ref. 4 for the Auger transition moments between initial- and final-state many-particle (CI) wave functions built on sets of mutually nonorthogonal orbitals

$$A_{fi}=\sum_x(\langle\nu\,|\,H_1\,|\,x\rangle-E\langle\nu\,|\,x\rangle)\langle\psi_f^{N-2}\,|\,\hat{a}_x\,|\,\psi_{1s}^{N-1}\rangle$$
$$+\tfrac{1}{2}\sum_{h,x,y}(\langle\nu h\,|\,xy\rangle-\langle\nu h\,|\,yx\rangle)$$
$$\times\langle\psi_f^{N-2}\,|\,\hat{a}_h^{\dagger}\hat{a}_x\hat{a}_y\,|\,\psi_{1s}^{N-1}\rangle \qquad (14)$$

although the full expression has not been implemented computationally. The notations are here the same as in Sec. II; H_1 denotes the one-electron Hamiltonian. The formulation in Eq. (14) assumes a single-channel strong orthogonal continuum function for the Auger electron and thus neglects continuum interaction between the channels.

For uncorrelated wave functions Eq. (14) reduces to the one already given by Howat, Åberg, and Goscinski[3] for unrestricted spin-orbitals and to the expressions given in Appendix A in the spin-restricted case. Using, on the other hand, orthogonal orbitals but retaining many-particle (CI) wave functions throughout, Eq. (14) reduces to

$$A_{fi}=\tfrac{1}{2}\sum_{h,x,y}\tau_{hxy}\chi_{hxy}\ , \qquad (15)$$

where τ_{hxy} and χ_{hxy} denote the Auger transition moment and the generalized Auger overlap amplitude (GAOA), respectively. Approximating furthermore the initial state with a single Slater determinant the intensity (squared transition amplitude) reduces to

$$I_{fi}=|\,A_{fi}\,|^2\propto\left|\sum_{x,y}\tau_{hxy}c_{xy}\right|^2. \qquad (16)$$

where c_{xy} are the expansion coefficients of the (x,y) configuration functions in the final state. These coefficients (equal to the pole strength of the particle-particle Green's function[6]) give the weights of the specific independent channels to the interacting channel rates. Results from

TABLE IV. Intensities of Auger transitions in the water molecule. Comparison between results from atomic decomposition (Ref. 7), mixed-wave, and hole-mixing calculations.

Channel	Atomic decomposition (arb. units)	Mixed wave (10^{-6} a.u.)	Mixed wave (arb. units)	Hole mixing (10^{-3} a.u.)	Hole mixing (arb. units)
$2a_1^{-2}$ S	48	593	96	354	61
$2a_13a_1$ S	48	467	76	374	65
$2a_13a_1$ T	11	177	29	166	29
$2a_11b_2$ S	32	318	51	258	45
$2a_11b_2$ T	8	141	23	119	21
$2a_11b_1$ S	55	414	67	335	58
$2a_11b_1$ T	14	197	32	164	28
$3a_1^{-2}$ S	71	440	71	393	68
$3a_11b_2$ S	58	569	92	557	96
$3a_11b_2$ T	1	9	1	9	2
$3a_11b_1$ S	99	624	101	593	102
$3a_11b_1$ T	2	12	2	11	2
$1b_2^{-2}$ S	34	358	58	345	60
$1b_21b_1$ S	74	553	89	533	92
$1b_21b_1$ T	0	0	0	0	0
$1b_1^{-2}$ S	100	618	100	579	100

the implementation of Eqs. (16) and (A2) are discussed below.

1. Relaxation

Auger rates computed by Wentzel's ansatz may show a marked dependence on the orbital basis set used for the initial and final states. For neon Howat, Åberg, and Goscinski[3] found a variation in the order of 10% of the Auger rates, depending on whether relaxed (mutually nonorthogonal) orbital basis sets were used or not. In order to test this effect for the water spectrum we computed the Auger rates corresponding to channel $3a_1^{-2}$ [partial wave (2,0)], channel $1b_2^{-2}$ [partial wave (2,2)], and channel $1b_1^{-2}$ [partial wave (2,2)], using final-state relaxed bound orbitals, obtained by double-hole SCF calculations. The results are collected in column B of Table I, while in column A the same quantities obtained by using neutral ground-state bound orbitals for the final states are reported for comparison. As already mentioned, the Auger rate expressions in Eq. (10) must be considered to be a first-order approximation to (9). A more correct expansion, retaining the lowest-order contributions deriving from the nondiagonal orbital overlap, is Eq. (A2) in Appendix A. This expression was computed exactly for the three test calculations mentioned above; the results are collected in the last column of Table I. The largest effect is that due to electronic relaxation. However, the percent variation of the Auger rate is relatively small, less than $+8\%$ for the three considered channels, and is partially compensated for by the variation due to the inclusion of nondiagonal overlap elements that are negative. The increase of the Auger rates by using final-states relaxed orbitals is clearly explainable. Because electronic relaxation due to holes in the valence shell of H_2O does not change the bound orbitals in a marked way, the effect on the one-electron Hamiltonian in Eqs. (7) and (8), and therefore on the continuum orbital, is negligible. More important is the contraction of the $1s$ orbital, which, even if very small, can increase the value of the two-electron integrals in Eq. (10) significantly. On the other hand, the direct overlap factor $\langle v \mid v' \rangle$ between core-hole and valence two-hole optimized orbitals has the opposite effect of reducing the channel rates. The effect is small for water and probably for other "atomiclike" systems, due to nearly unit overlap matrices (cf. Table V). For general molecules with more easily polarizable bonds such as for unsaturated systems, this overlap effect becomes important.

TABLE V. Molecular orbital overlap matrix between ground- and core-hole state optimized orbitals.

	$1a_1$	$2a_1$	$3a_1$	$1b_2$	$1b_1$
$1a_1$	0.999	−0.006	0.002	0.0	0.0
$2a_1$	0.008	0.993	−0.013	0.0	0.0
$3a_1$	−0.002	0.007	0.980	0.0	0.0
$1b_2$	0.0	0.0	0.0	0.982	0.0
$1b_1$	0.0	0.0	0.0	0.0	0.980

2. Configuration interaction and hole-mixing

Weighting coefficients, channel intensities, and energies obtained from the CI calculations are given in Tables II and VI. We can divide the Auger channels in three types according to the nature of their discrete-state interaction: the $2a_1^{-2}$ (inner-inner valence) state, the $2a_1^{-1}v^{-1}$ containing states (inner-outer valence), and states which are $2p^{-2}$ based (outer-outer valence). The non-totally-symmetric states of the latter group are well described within the independent-particle approximation. The interaction for these is of dynamical character, represented in the CI picture by external single and double excitations which act as a slight modulation of the single leading GAOA in the intensity expression, Eq. (16). For the totally symmetric states there is a rather strong internal configuration interaction, between main two-hole configuration state functions (CSF's), which already has been stated in a previous investigation using internal CI wave functions.[25] This interaction gives rise to hole-mixing effects,[4] and the calculation of interacting rates therefore also requires the phases of the Auger transition moments τ_{hxy} (for deter-

TABLE VI. Partial and total Auger channel rates obtained from hole-mixing calculations (10^{-6} a.u.).

Channel		(0,0)	(1,−1)	(1,0)	(1,1)	(2,−2)	(2,−1)	(2,0)	(2,1)	(2,2)	Sum
$2a_1^{-2}$	S	344		10				0		0	354
$2a_13a_1$	S	117		247				9		1	374
$2a_13a_1$	T	0		166				0		0	166
$2a_11b_2$	S		252				6				258
$2a_11b_2$	T		119				0				119
$2a_11b_1$	S				324				11		335
$2a_11b_1$	T				164				0		164
$3a_1^{-2}$	S	23		19				320		31	393
$3a_11b_2$	S		20				537				557
$3a_11b_2$	T		9				0				9
$3a_11b_1$	S				27				566		593
$3a_11b_1$	T				11				0		11
$1b_2^{-2}$	S	140		2				42		161	345
$1b_21b_1$	S					533					533
$1b_21b_1$	T					0					0
$1b_1^{-2}$	S	77		1				175		326	579
Total											4790

mination of phases see Sec. III).

For states containing the inner valence ($2a_1$) hole there is some mixing between the $2a_1^{-1}v^{-1}$ and $3a_1^{-1}v^{-1}$ CSF's. Weak satellite transitions with small GAOA's are associated with these transitions. The $2a_1^{-2}$ state, finally, is very strongly affected by semi-internal interaction which shifts the main transition energy as much as 6 eV.[26] The semi-internal interaction originates in resonances between negative internal excitations with external excitations. It is similar to, but much stronger than, the "breakdown of the molecular orbital" effect in the inner-valence photoelectron spectrum of H_2O.[30,31] A difference between the Auger spectrum of H_2O and of first-row diatomics is that for the latter the MO breakdown is present over a wide energy interval, which also covers the inner-outer valence hole states.[10]

Figure 3 displays a bar spectrum of CI transition energies (Table II) and hole-mixing intensities along with the experimental recording.[7] The intensities were obtained as weighted partial-wave intensities according to Eq. (16). Using an identical orbital set for initial and final states, the rates are given by the computable expression Eq. (16) if the initial state is approximated by the main Slater determinant. The expansion coefficient of this determinant was 0.88 for GS optimized but as big as 0.98 for core-state-optimized orbitals. On the other hand, as shown above, the nonorthogonality contributions to the rates obtained from single CSF's are small, and the expansion coefficients (GAOA's) displayed in Table II can therefore to a rather good approximation be taken as a guide for the effect of discrete-state channel interaction. The role of initial-state correlation (many-determinant core-hole state wave function) becomes increasingly more important towards the low-kinetic-energy end of the spectrum, where discrete final-state interaction is strong and the weight of the leading GAOA is diminished. For these states, "excited" initial-state determinants will have nonnegligible Auger overlap amplitudes with excited final-states determinants and the validity of Eq. (16) used to construct the final hole-mixing intensities (Fig. 3) becomes accordingly more limited.

C. Lifetime broadening of the core 1s state

Since the fluorescence yield of core-hole states of first-row elements is very small, the lifetime broadening is directly given by the total Auger rate. Our computed values for the total rate and the lifetime broadening for the core $1s$ state of H_2O were 5.5×10^{-3} and 0.15 eV, respectively, using mixed-wave calculations of the individual channel rates (the sum of the partial channel rates is only slightly larger). Except for the work of Faegri and Kelly on HF (Ref. 11) there are no *ab initio* values for molecular core-decay rates available. No entries for the oxygen atom is found in the compilation of Krause,[27] neither is the core-electron spectrum of water sufficiently resolved vibrationally to allow for a determination of the core-state lifetime.[28] Our value fits, however, into the trend given by near-lying Z elements in Krause's tables. The two main sources of errors to this value are counteracting: (i) there is an increase of the lifetime width due to interaction between the core state with continua of ionic states with charge higher than 2, and (ii) a decrease due to many-body effects for the main channels. The correlated total rate in Table VI does not include satellite rates, however, even with their inclusion the total rate decreases [cf. intensity model given by Eq. (16)], which is in agreement with Kelly's many-body perturbation theory calculations on neon.[5] We expect that the effect of discrete and continuum channel interaction is not so important for the total rate as it might be for the individual channel rates, see also results by Howat, Åberg, and Goscinski for neon.[3] In a future publication we investigate the nuclear variation of core-hole decay rate, and explore the effects of this variation on the band-shape formation in emission-type spectra of H_2O.[29]

V. CONCLUSIONS

In the present work we have derived and implemented a Stieltje's imaging method for calculations of Auger transition rates which accounts for the full anisotropy of the molecular ionic field. Moments, total and separate channel cross sections for the Auger decay have been evaluated at different levels of approximation, viz., partial-wave, mixed-wave, and interacting-channel approximations. In connection with the study of channel interaction a detailed investigation on the role of relaxation (orbital nonorthogonality) and discrete configuration interaction was carried out. It is shown that the mixing of the partial waves is moderate for the Auger spectrum of the water molecule, while discrete channel interaction (breakdown of the molecular orbital picture and hole-mixing effects) is essential especially towards the high-kinetic-energy part of the spectrum. The square-integrable basis set of Slater and trigonometric functions describes excellently the electron continuum over a wide energy range and despite their character of being resonant at high kinetic energies the Auger moments are found to be stable towards variations in this basis.

The presently devised techniques can straightforwardly be extended for studies on the validity of the "constant-resonance-width approximation" for inner vacancy states, i.e., for calculation of the nuclear variation of the lifetime, as well as for the calculation of the electronic energy shift for a metastable molecular state due to the discrete-continuum interaction. Such work is now in progress. concerning two other aspects of molecular Auger not covered by the present study, namely, the full coupling of the continuum parts of the separate channels and the angular distribution of the Auger electrons, we foresee a need for a detailed consideration of the molecular scattering states.

ACKNOWLEDGMENTS

The authors would like to thank Dr. I. Cacelli who kindly supplied part of the computer code employed in the present work, and Hans Olofsson at the faculty of science computing center in Uppsala for provision of computer time. This work was supported by the Swedish Natural Science Research Council and by the Italian Consiglio Nazionale delle Ricerche.

APPENDIX A

In this appendix we present expressions for the Auger transition moments when initial and final states are represented by Slater determinants built on spin-orbital sets that are mutually nonorthogonal. For unrestricted spin-orbitals such expressions were given by Howat, Åberg, and Goscinski,[3]

$$\langle \psi_{xy\varepsilon} | \hat{H}-E | \psi_{1s} \rangle = \prod_{j\,(\neq x,y)} \langle j' | j \rangle \left[\langle \varepsilon' 1s' || xy \rangle + \begin{vmatrix} \langle \varepsilon' | J | x \rangle & \langle \varepsilon' | J | y \rangle \\ \langle 1s' | x \rangle & \langle 1s' | y \rangle \end{vmatrix} + \begin{vmatrix} \langle \varepsilon' | x \rangle & \langle \varepsilon' | y \rangle \\ \langle 1s' | J | x \rangle & \langle 1s' | J' | y \rangle \end{vmatrix} - \xi \begin{vmatrix} \langle \varepsilon' | x \rangle & \langle \varepsilon' | y \rangle \\ \langle 1s' | x \rangle & \langle 1s' | y \rangle \end{vmatrix} \right] + \sum_{j\,(\neq x,y)} \left[\begin{vmatrix} \langle i' | x \rangle & \langle i' | y \rangle \\ \langle \varepsilon' 1s' || xi \rangle & \langle \varepsilon' 1s' || yi \rangle \end{vmatrix} + \begin{vmatrix} \langle \varepsilon' | i \rangle & \langle 1s' | i \rangle \\ \langle \varepsilon' i' || xy \rangle & \langle 1s' i' || xy \rangle \end{vmatrix} \right], \tag{A1}$$

where

$$\langle ab||cd \rangle = \left\langle ab \left| \frac{1}{r_{12}} \right| cd \right\rangle - \left\langle ab \left| \frac{1}{r_{12}} \right| cd \right\rangle ,$$

$$J = H_1 + \sum_{j\,(\neq x,y)} \langle j'||j \rangle ,$$

$$\xi = E - \tfrac{1}{2} \sum_{j\,(\neq x,y)} (\langle j' | H_1 | j \rangle + \langle j' | J | j \rangle) .$$

H_1 is the one-electron Hamiltonian and the apex marks the final-state spin-orbitals. In the case of Auger transitions leading to double ionization in the same shell Eq. (A1) takes the following spin-restricted form:

$$\langle \psi_{xy\varepsilon} | \hat{H}-E | \psi_{1s} \rangle = \prod_{j \begin{bmatrix} \neq x \\ \neq 1s \end{bmatrix}} (j' | j)^2 (1s' | 1s) \Big\{ (\varepsilon' x \mid 1s' x) + (1s' | x) F_{\varepsilon' x} + (\varepsilon' | x) F_{1s' x} - A_x (\varepsilon' | x)(1s' | x) - \sum_{j\,(\neq x)} [(j' | x)(\varepsilon' j \mid 1s' x) + (\varepsilon' | j)(1s' x \mid j' x)] - \sum_{j \begin{bmatrix} \neq x \\ \neq 1s \end{bmatrix}} [(j' | x)(\varepsilon' x \mid 1s' j) + (1s' | j)(\varepsilon' x \mid j' x)] \Big\} \tag{A2}$$

with

$$F_{a' x} = (a' | H_1 | x) + \sum_{j \begin{bmatrix} \neq x \\ \neq 1s \end{bmatrix}} [2(j' j \mid a' x) - (j' x \mid a' j)] + (1s' 1s \mid a' x) ,$$

$$A_x = E - 2 \sum_{j \begin{bmatrix} \neq x \\ \neq 1s \end{bmatrix}} (j' | H_1 | j) - (1s' | H_1 | 1s) - \sum_{i \begin{bmatrix} \neq x \\ \neq 1s \end{bmatrix}} \sum_{j\,(\neq x)} [2(i' i \mid j' j) - (i' j \mid j' i)] ,$$

where the two-electron integrals are defined by Eq. (11). Equation (A2) has been numerically implemented in order to test the importance of using relaxed final-state orbitals in the calculation of Auger moments (see discussion in Sec. IV B 1).

[1] T. Åberg and G. Howat, *Corpuscles and Radiation in Matter I*, Vol. 31 of *Handbuch der Physik* (Springer, Berlin, 1982).
[2] G. Wentzel, Z. Phys. **43**, 521 (1927).
[3] G. Howat, T. Åberg, and O. Goscinski, J. Phys. B **11**, 1575 (1978).
[4] R. Manne and H. Ågren, Chem. Phys. **93**, 201 (1985).
[5] H. P. Kelly, Phys. Rev. A **11**, 556 (1975).
[6] C. M. Liegener, Chem. Phys. **76**, 397 (1983).
[7] H. Siegbahn, L. Asplund, and P. Kelfve, Chem. Phys. Lett. **35**, 330 (1975).
[8] H. Ågren and H. Siegbahn, Chem. Phys. Lett. **72**, 424 (1980).
[9] O. M. Kvalheim and K. Faegri, Chem. Phys. Lett. **67**, 127 (1979).
[10] H. Ågren, J. Chem. Phys. **75**, 1267 (1981).

[11]K. Faegri and H. P. Kelly, Phys. Rev. A **23**, 52 (1981).
[12]M. Hihashi, E. Hiroike, and T. Nakajima, Chem. Phys. **68**, 377 (1982).
[13]*Electron-Molecule and Photon-Molecule Collisions,* edited by T. Rescigno, V. McKoy, and B. Schneider (Plenum, New York, 1979).
[14]P. W. Langhoff and C. T. Corcoran, J. Chem. Phys. **61**, 146 (1974).
[15]P. W. Langhoff, C. T. Corcoran, J. S. Sims, F. Weinhold, and R. M. Glover, Phys. Rev. A **14**, 402 (1976).
[16]T. N. Rescigno, C. F. Bender, B. V. McKoy, and P. W. Langhoff, J. Chem. Phys. **68**, 970 (1978).
[17]G. H. F. Diercksen, W. P. Kraemer, T. N. Rescigno, C. F. Bender, B. V. McKoy, S. R. Langhoff, and P. W. Langhoff, J. Chem. Phys. **76**, 1043 (1982).
[18]I. Cacelli, R. Moccia, and V. Carravetta, Chem. Phys. **90**, 313 (1984).
[19]I. Cacelli, V. Carravetta, and R. Moccia, J. Phys. B **18**, 1375 (1985).
[20]I. Cacelli, R. Moccia, and V. Carravetta, in *Collisions and Half-Collisions with Lasers,* edited by N. K. Rahman and C. Guidotti (Harwood Academic, New York, 1984), p. 229.
[21]R. L. Chase, H. P. Kelly, and H. S. Köhler, Phys. Rev. A **3**, 1550 (1971).
[22]H. P. Kelly, in *Atomic Inner-Shell Processes,* edited by B. Crasemann (Academic, New York, 1975), p. 331.
[23]P. E. M. Siegbahn, J. Chem. Phys. **75**, 2314 (1981).
[24]H. J. Aa. Jensen and H. Ågren, Chem. Phys. Lett. **110**, 140 (1984); Chem. Phys. **102**, 256 (1986).
[25]H. Ågren, S. Svensson, and U. I. Wahlgren, Chem. Phys. Lett. **35**, 336 (1975).
[26]H. Ågren and H. Siegbahn, Chem. Phys. Lett. **69**, 424 (1980).
[27]M. O. Krause, J. Chem. Phys. Data **8**, 307 (1979).
[28]K. Siegbahn, J. Electron. Spectrosc. **5**, 3 (1974).
[29]H. Ågren, A. Flores-Riveros, and V. Carravetta (unpublished).
[30]L. S. Cederbaum, Mol. Phys. **28**, 479 (1974).
[31]V. Carravetta and R. Moccia, Mol. Phys. **35**, 129 (1978).